Science of the Total Environment 799 (2021) 149357

Contents lists available at ScienceDirect

Science of the Total Environment

journal homepage: www.elsevier.com/locate/scitotenv

The impact of the abnormal salinity enrichment in pore water on the thermodynamic stability of marine natural gas hydrates in the Arctic region

Wonjung Choi [a,1], Joonseop Lee [a,1], Young-Gyun Kim [b], Hanwoong Kim [a], Tae Siek Rhee [c], Young Keun Jin [d], Ji-Hoon Kim [e], Yongwon Seo [a,*]

[a] Department of Urban and Environmental Engineering, Ulsan National Institute of Science and Technology, 50 UNIST-gil, Ulju-gun, Ulsan 44919, Republic of Korea
[b] Research Institute of Earth Resources, Kangwon National University, 1 Gangwondaehak-gil, Chuncheon-si, Gangwon-do 24341, Republic of Korea
[c] Division of Polar Ocean Sciences, Korea Polar Research Institute, 26 Songdomirae-ro, Yeonsu-gu, Incheon 21990, Republic of Korea
[d] Division of Polar Earth-system Sciences, Korea Polar Research Institute, 26 Songdomirae-ro, Yeonsu-gu, Incheon 21990, Republic of Korea
[e] Division of Petroleum and Marine Resources Research, Korea Institute of Geoscience and Mineral Resources, 124 Gwahak-ro, Yuseong-gu, Daejeon 34312, Republic of Korea

HIGHLIGHTS

- NGHs from ARAON Mounds were composed of mostly CH_4 and found to be sI.
- Saturation of NGHs in ARAON Mounds was determined to be ~35%.
- Abnormal salinity enrichment was observed in the residual pore water of the sediment.
- Salinity enrichment could induce NGH dissociation at a lower temperature than expected.

GRAPHICAL ABSTRACT

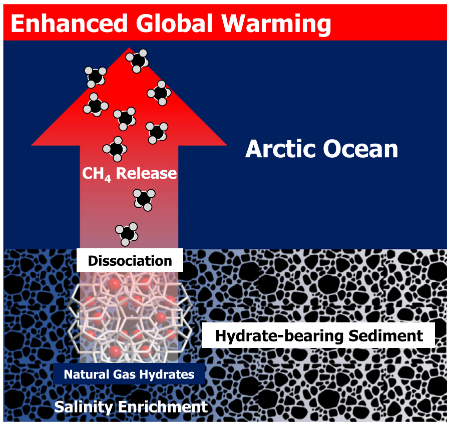

ARTICLE INFO

Article history:
Received 21 May 2021
Received in revised form 13 July 2021
Accepted 26 July 2021
Available online 30 July 2021

Editor: Christian Herrera

Keywords:
Natural gas hydrates
Arctic

ABSTRACT

In this study, the thermodynamic and structural characteristics of natural gas hydrates (NGHs) retrieved from gas hydrate mounds (ARAON Mound 03 (AM03) and ARAON Mound 06 (AM06)) in the Chukchi Sea in the Arctic region were investigated. The gas compositions, crystalline structure, and cage occupancy of the NGHs at AM03 and AM06 were experimentally measured using gas chromatography (GC), ^{13}C nuclear magnetic resonance (NMR), Raman spectroscopy, and powder X-ray diffraction (PXRD). In the NGHs from AM03 and AM06, a significantly large fraction of CH_4 (> 99%) and a very small amount of H_2S were enclathrated in small (5^{12}) and large ($5^{12}6^2$) cages of sI hydrate. The NGHs from AM03 and AM06 were almost identical in composition, guest distributions, and existing environment to each other. The salinity of the residual pore water in the hydrate-bearing sediment (AM06) was measured to be 50.32‰, which was much higher than that of seawater (34.88‰). This abnormal salinity enrichment in the pore water of the low-permeability sediment might induce the dissociation of NGHs at a lower temperature than expected. The saturation changes in the NGHs that corresponded with an

---

* Corresponding author.
E-mail address: ywseo@unist.ac.kr (Y. Seo).
[1] These authors contributed equally to this work.

https://doi.org/10.1016/j.scitotenv.2021.149357
0048-9697/© 2021 Elsevier B.V. All rights reserved.

Salinity
Structure I
Thermodynamic stability
Saturation

increase in the seawater temperature were also predicted on the basis of the salinity changes in the pore water. The experimental and predicted results of this study would be helpful for understanding the thermodynamic stability of NGHs and potential CH_4-releasing phenomena in the Arctic region.

© 2021 Elsevier B.V. All rights reserved.

1. Introduction

Gas hydrates are solid-state crystalline compounds composed of guest gas molecules and hydrogen-bonded host water molecules, which are stabilized by van der Waals force between guest and host molecules generally under low temperature and high pressure conditions (Sloan and Koh, 2007). Naturally occurring gas hydrates can be found in ocean sediments and beneath terrestrial permafrost regions where the thermodynamic conditions for the formation of gas hydrates are satisfied (Kvenvolden and Lorenson, 2001). Because of their enormous deposits around the world, natural gas hydrates (NGHs) have received great attention as our future clean energy resources and in the global carbon cycle. (Pinero et al., 2013; Wu et al., 2021). NGHs with three different structures (structure I (sI), structure II (sII), and structure H (sH)) have been discovered in nature depending on their guest compositions and surroundings (Sloan and Koh, 2007).

Various NGH samples have been successfully collected from marine environments through previous explorations (Sahu et al., 2020). The most common NGH structure in nature is sI which has been discovered all over the world, including the Nankai Trough (Japan), the South China Sea (China), the Ulleung Basin (S. Korea), and the Arctic region (Bahk et al., 2013; Jin et al., 2016; Li et al., 2018; Marín-Moreno et al., 2016). Recent investigation also revealed the existence of sII and sH hydrates at the Cascadia margin (Canada), the South China Sea (China), and the Gulf of Mexico (USA) (Fang et al., 2019; Klapp et al., 2010; Lu et al., 2007; Wei et al., 2018; Wei et al., 2019; Wei et al., 2021). NGHs with sII and sH have higher thermodynamic stability due to the inclusion of large hydrocarbon molecules; accordingly, they can exist at a shallower depth compared to NGHs with sI, which might result in easier access and more feasible production (Holder et al., 1987; Lee et al., 2021; Li et al., 2018; Ye et al., 2019). Because natural gas production from NGHs would be influenced by the structure of the NGHs, a comprehensive understanding of the characteristics of target NGHs is required for successful exploration and production (Choi et al., 2020a; Choi et al., 2020b).

The amount of NGH deposits in the Arctic region was estimated to be approximately 6621 trillion cubic feet, which indicates that the Arctic region is one of the most abundant sources for NGHs in the world (Max et al., 2013). Previous studies on the Artic hydrates revealed that CH_4 is the major component and the guest CH_4 molecules of the Artic hydrates have either a thermogenic or a biogenic origin based on the isotopic data of hydrocarbon gas (Kim et al., 2020a; Pape et al., 2020). The morphology and crystalline structure of some NGHs in the Arctic region were also examined using a scanning electron microscope and X-ray diffraction (Gamboa et al., 2017; Stern et al., 2011). However, these Arctic hydrates, which are regarded as our future clean energy resources, might cause a serious problem due to an uncontrolled emission of CH_4, which has a 28 times greater global warming potential than that of CO_2 (Biastoch et al., 2011; Maslin et al., 2010). This CH_4-releasing phenomenon, which has been frequently observed in the Arctic region, could seriously accelerate global warming (MacDougall et al., 2012; Wallmann et al., 2018).

On the other hand, various types of salts are included in seawater and they can act as thermodynamic hydrate inhibitors that disrupt hydrogen bonds of water molecules (Dickens and Quinby-Hunt, 1994). As revealed in the hydrate-based desalination process, the salinity of residual fluid increases as gas hydrate formation proceeds in a closed system because salt ions are excluded from hydrate crystals and released into fluid (Choi et al., 2019; Mok et al., 2021). Salt enrichment can similarly occur in the pore water of hydrate-bearing sediments with low permeability (Almenningen et al., 2018; Kim et al., 2013; Ruppel et al., 2005). The presence of low-permeability sediments that consist of mud or fine grains has been confirmed in the Arctic region through previous expeditions (Gründger et al., 2019; Kim et al., 2020b). Because the thermodynamic stability of NGHs in sediment can be largely influenced by salinity, a close investigation into the salinity in pore water of hydrate-bearing sediments is essential for gaining insight into the gas hydrate stability zone and the potential CH_4-releasing behavior in the Arctic region. However, previous studies have not considered the concentration gradient of salinity or the salt enrichment in pore water for prediction and estimation of gas hydrate stability in the Arctic region (Hong et al., 2017; Serov et al., 2017).

In this study, the precise nature and unique patterns of NGH samples from ARAON Mounds (ARAON Mound 03 (AM03) and ARAON Mound 06 (AM06)) in the Chukchi Sea during ARA09C and ARA10C Expeditions were experimentally investigated to understand NGHs as both clean energy resources and emission sources for global warming. The guest compositions of the NGH samples were directly measured using gas chromatography. The cage-specific guest occupancy, crystalline structure, and weight fractions of the NGH samples were analyzed via nuclear magnetic resonance (NMR), Raman spectroscopy, and powder X-ray diffraction (PXRD). In addition, the salinity of pore water in hydrate-bearing sediments was examined to determine the influence of salinity changes caused by the formation and dissociation of gas hydrates on the thermodynamic stability of NGHs.

2. Materials and methods

2.1. In-situ salinity and temperature measurement and hydrate sampling

The salinity and temperature on the top of ARAON Mounds (AMs) in the Chukchi Sea were measured using a conductivity-temperature-depth (CTD, SBE 911plus) system onboard Ice-Breaking Research Vessel (IBRV) ARAON (Hahm et al., 2015). As shown in Fig. 1(a), CTD data were obtained 10 m above seven mounds (AM00, AM01, AM02, AM03, AM04, AM06, and AM07). The bottom of the ridge was designated as AM00. The locations and depths for the CTD data used in this study are presented in Fig. 1(b). The NGH samples were successfully retrieved from AM03 and AM06 in 2018 and 2019, respectively, using a gravity corer (GVC). The collected NGH samples were stored in a cryogenic dry shipper (21XT-Al, Taylor Wharton, USA) filled with liquid nitrogen to prevent the dissociation of NGHs. The images of split sediment cores from AM03 and AM06 are shown in Fig. 1(c). The detailed locations of each AM and the measured temperature and salinity values at each AM are summarized in Table 1.

2.2. Gas chromatography (GC)

To measure the composition of guest molecules in the NGH samples, powdered NGH samples were annealed at 93 K for 30 min to evaporate residual liquid nitrogen which was used for storage of NGH samples. The dried NGH samples were then dissociated inside a syringe that was connected to a Tedlar gas sampling bag for collecting gas retrieved from NGH samples. The compositions of the retrieved gas were measured using the 490 Micro GC system (Agilent, USA) equipped with dual thermal conductivity detectors coupled to a CP-Molsieve 5 Å column (Agilent, USA) and a CP-PoraPLOT Ucolumn (Agilent, USA). Composition measurements were repeated three times and the averaged values were provided.

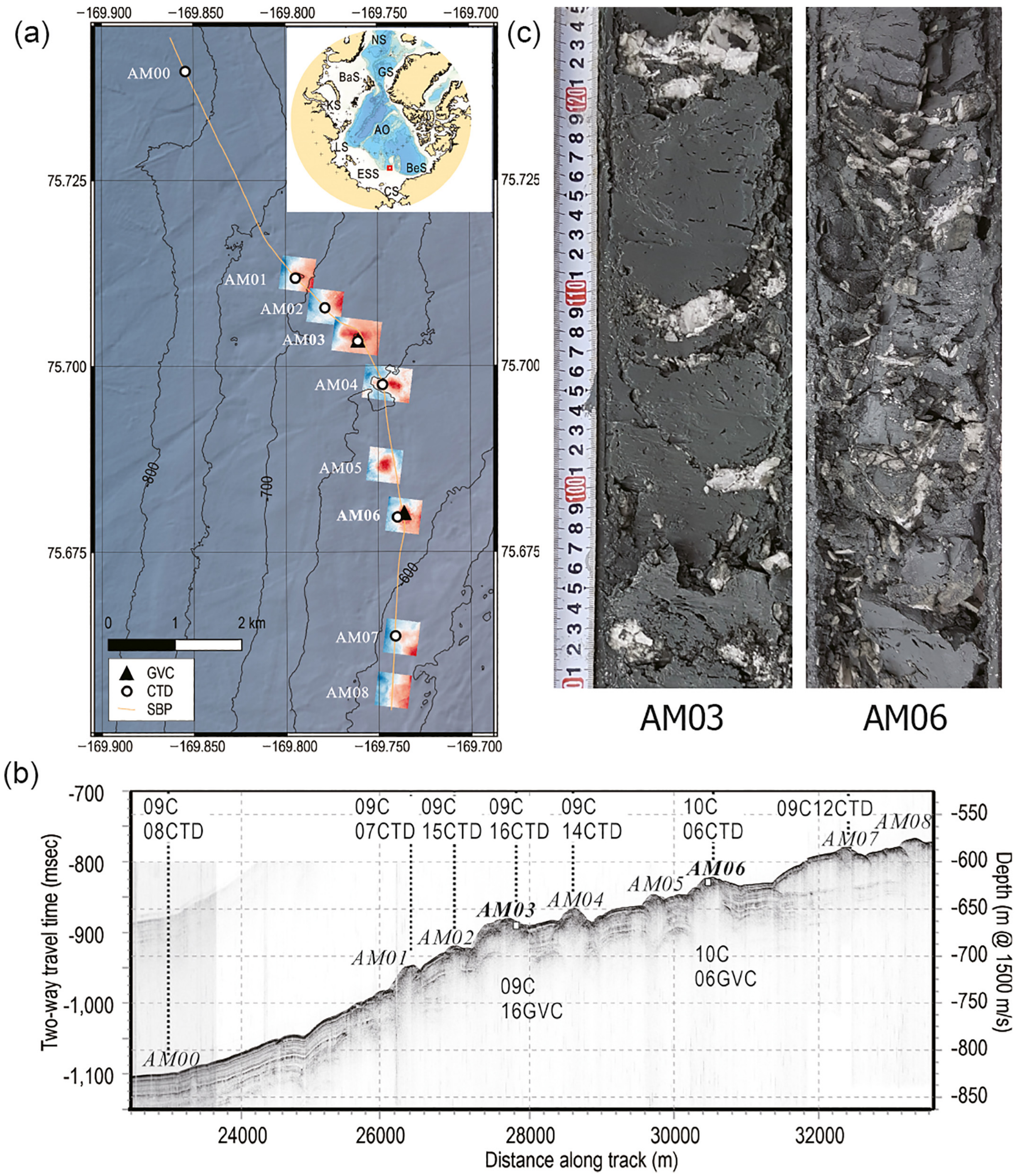

Fig. 1. (a) A map of sampling locations of AMs for CTD and GVC, (b) sub-bottom profile of AMs, and (c) images of split sediment cores from AM03 and AM06.

2.3. Nuclear magnetic resonance (NMR) spectroscopy

For NMR measurement, the NGH samples were ground into fine particles less than 50 μm using a micro sieve in a liquid nitrogen container. ^{13}C NMR spectra were collected using a Bruker 400 MHz solid-state NMR spectrometer from the Korea Basic Science Institute (KBSI) at a Larmor frequency of 100.6 MHz with a magic angle spinning (MAS) of 2–4 KHz. Finely powdered hydrate samples were loaded into a 4 mm O.D. Zr rotor, which was then placed in a variable-temperature probe at 213 K. The downfield carbon resonance peak of adamantane (38.3 ppm at 300 K) was utilized as an external chemical shift reference.

Table 1
Sampling locations of AMs for CTD and GVC/temperature and salinity values at the given depth of each AM.

Mound	Latitude (N)	Longitude (W)	Depth (m)	Temperature (K)	Salinity (‰)	NGHs	Remarks
AM00	75° 44.38′	169° 51.26′	805.7	273.7	34.88	–	ARA09C
AM01	75° 42.71′	169° 47.68′	694.1	273.8	34.88	–	ARA09C
AM02	75° 42.47′	169° 46.72′	671.2	273.8	34.88	–	ARA09C
AM03	75° 42.20′	169° 45.65′	643.0	273.9	34.88	Gained	ARA09C
AM04	75° 41.85′	169° 44.85′	631.7	273.6	34.88	–	ARA09C
AM06	75° 40.77′	169° 44.16′	598.0	274.0	34.88	Gained	ARA10C
AM07	75° 39.82′	169° 44.46′	571.4	274.0	34.88	–	ARA09C

2.4. Raman spectroscopy

A micro-Raman spectrometer (alpha 300R, WITec, Germany) with a thermoelectrically cooled CCD detector and a 1800 grooves/mm holographic grating was used to observe the enclathrated guest molecules. The cylindrically pelletized samples were prepared for Raman measurement. The Raman spectra were obtained at 93 K under atmospheric pressure in the range of 1200–1300 cm^{-1} and 2500–2940 cm^{-1} to detect enclathrated guest molecules.

2.5. Powder X-ray diffraction (PXRD)

The PXRD patterns of finely powdered NGH samples were obtained from the 6D beamline at the Pohang Accelerator Laboratory (Republic of Korea). The diffraction patterns were collected with an exposure time of 100 s at 133 K and an energy of 12.658 keV ($\lambda = 0.9795$ Å). The two-dimensional patterns (Q-spacing, nm^{-1}) obtained were converted to one-dimensional diffraction patterns with an energy of 8.0475 keV. The obtained PXRD patterns were analyzed through the profile-matching and Rietveld methods using the FullProf program to represent the crystalline structure, lattice parameters, weight fractions, and cage occupancy of the NGH samples.

2.6. Salinity measurement

The salinity of gas hydrates and that of pore water were separately measured in this study. The salinity of the NGH samples, here referring to NaCl concentration in solution, was measured using an Orion Star conductivity benchtop meter (A212, ThermoScientific, USA) that was calibrated using two standard solutions of 1413 mS/cm (692 ppm as NaCl; Orion 011007) and 12.9 mS/cm (7230 ppm as NaCl; Orion 011006). To measure the salinity of the gas hydrate phase, several pieces of the solid hydrate from the bulk NGH samples were collected; the collected pieces were then dissociated to obtain the solution from the hydrate. On the other hand, the salinity of pore water in the hydrate-bearing sediments was measured after some collected sediment samples were diluted in a predetermined amount of deionized water. A more detailed description of the experimental methods and procedures used here is available in our previous papers (Kim et al., 2016; Lee et al., 2017).

3. Results and discussion

NGHs are known to be composed of various guest molecules depending on their locations and environments, and guest compositions of NGHs mainly affect their thermodynamic and structural characteristics (Kvenvolden and Lorenson, 2001). Fig. 2 represent the gas compositions of the NGHs collected from the bottom of the gravity cores in AM03 and AM06. CH_4 was a main component of the NGH samples (> 99%) at both AM03 and AM06, whereas the composition of H_2S and CO_2 was less than 1%. As seen in Fig. 1(c), since the volume expansion by the dissociation of NGHs was not observed in the split cores, the possible dissociation of NGHs during the sampling process was reasonably ignored in this study. From compositional analysis, the NGH samples at both AM03 and AM06 were expected to be sI hydrates due to the extremely high CH_4 concentration and the absence of hydrocarbons with longer chains like propane, isobutane, and *n*-butane.

Cage-dependent chemical shifts of enclathrated guest molecules in the ^{13}C MAS NMR spectra of gas hydrates enable us to identify the gas hydrate structure (Lee et al., 2013). The guest distributions can be quantified through the integration of resonance peaks for enclathrated guest molecules. Fig. 3 illustrates the ^{13}C NMR spectra of CH_4 hydrate, NGH at AM03, and NGH at AM06. The CH_4 hydrate exhibited two resonance peaks at −4.3 and −6.6 ppm which correspond to CH_4 molecules captured in the small (5^{12}) and large ($5^{12}6^2$) cages of sI hydrate, respectively. NGHs at both AM03 and AM06 also demonstrated two resonance peaks at −4.3 and −6.6 ppm in the range of 0 - −10 ppm.

The cage occupancy of guest molecules in gas hydrates can be calculated by combining statistical thermodynamic equations and relative areas of guest molecules from the ^{13}C NMR spectra (Seo and Lee, 2003). However, because the relative areas of H_2S and CO_2 were not available in this study, the cage occupancy ratios (θ_l/θ_s) of the large ($5^{12}6^2$) and small (5^{12}) cages for enclathrated CH_4 molecules were obtained instead of the specific cage occupancy. The θ_l/θ_s of the CH_4 hydrate was 1.07 (Mok et al., 2020), the θ_l/θ_s of the NGH at AM03 was 1.06, and the θ_l/θ_s of the NGH at AM06 was 1.03. The NGHs at AM03 and AM06 had slightly smaller θ_l/θ_s values than that of CH_4 hydrate. This was attributable to the slightly higher occupancy of H_2S and CO_2 in the large ($5^{12}6^2$) cages than in the small (5^{12}) cages of the NGHs at AM03 and AM06. The similar θ_l/θ_s values between the NGH at AM03 and the NGH at AM06 imply that the NGHs at AM03 and AM06 have similar compositions, guest distributions, and existing environments.

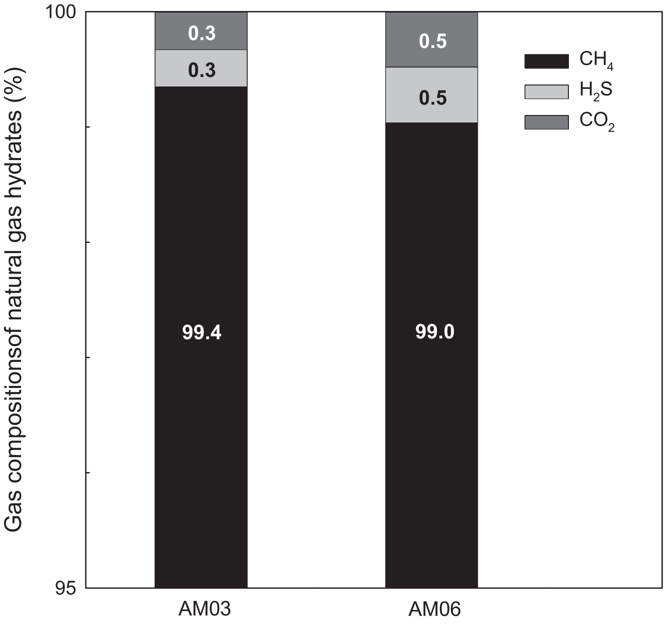

Fig. 2. Gas compositions of the NGH samples retrieved from AM03 and AM06.

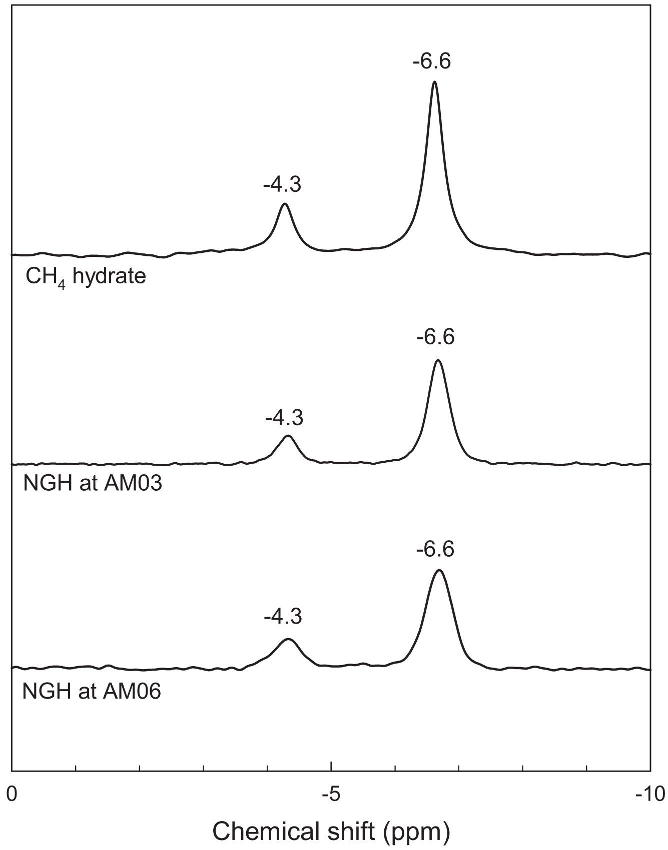

Fig. 3. ^{13}C NMR spectra of CH_4 hydrate, NGH at AM03, and NGH at AM06.

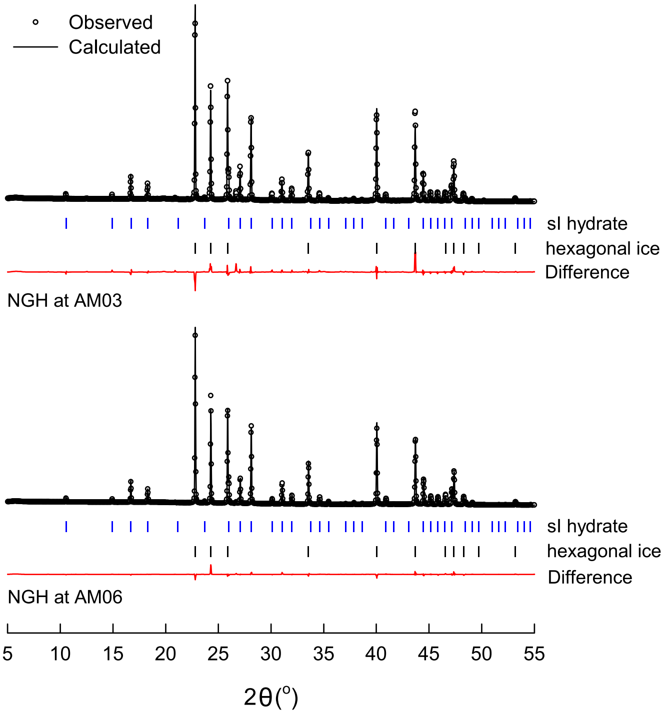

Fig. 5. PXRD patterns of NGHs at AM03 and AM06.

The inclusion of H_2S and CO_2 in the NGH samples could not be confirmed via ^{13}C NMR spectroscopy despite their possible presence in the cages of NGHs. Raman spectroscopy, which is another powerful tool to identify the enclathration of guest molecules in specific cages, was employed in this study. Fig. 4 shows the Raman spectra of the NGHs at AM03 and AM06 in the ranges of 1200–1350 cm^{-1}, 2520–2640 cm^{-1}, and 2880–2940 cm^{-1}. The Raman peaks of enclathrated CO_2 molecules in sI hydrates are known to appear at 1276 and 1380 cm^{-1} (Uchida et al., 1995). However, no peaks were observed in the range of 1200–1350 cm^{-1} in Fig. 4 even though the compositional analysis demonstrated the presence of a small amount of CO_2 in the NGH samples, indicating that CO_2 might actually exist in the residual water, not in the cages of the NGHs. The three peaks at 2571, 2594, and 2606 cm^{-1} in the range of 2520–2640 cm^{-1} were associated with H_2S. The peak at 2571 cm^{-1} was assigned to HS^- ion, and the peaks at 2594 and 2606 cm^{-1} were assigned to H_2S molecules in the large ($5^{12}6^2$) and small (5^{12}) cages of sI hydrate, respectively (Chen et al., 2015; Peltzer et al.,

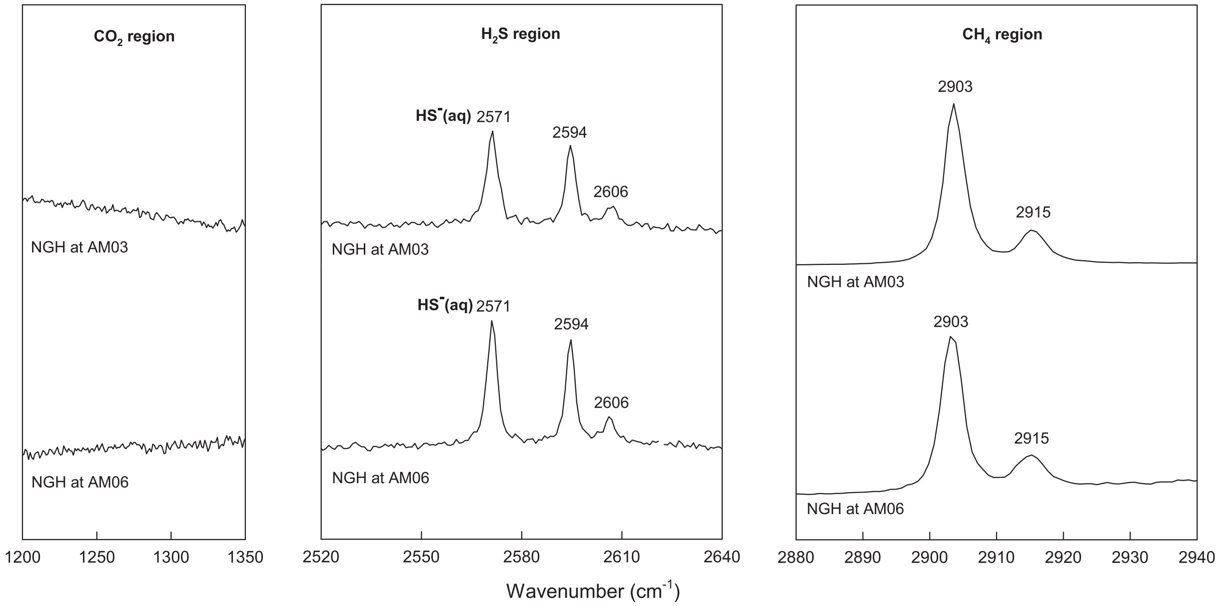

Fig. 4. Raman spectra of NGHs at AM03 and AM06.

Table 2
Summarized crystallographic information from Rietveld analysis of NGHs at AM03 and AM06.

Sample	Structure (space group)	Lattice parameter (Å)	Cage occupancy				Weight fraction (%)		R_{wp} (%)
			$\theta_{s,\ CH_4}$	$\theta_{l,\ CH_4}$	$\theta_{s,\ H_2S}$	$\theta_{l,\ H_2S}$	sI	Ih	
NGH at AM03	sI ($Pm\overline{3}n$)	11.8788(2)	0.8797	0.9364	0.0074	0.0076	36.3	63.7	14.4
NGH at AM06	sI ($Pm\overline{3}n$)	11.8654(1)	0.8755	0.9211	0.0075	0.0082	36.2	63.8	8.11

2016). The two peaks at 2903 and 2915 cm^{-1} originated from CH_4 molecules captured in the large ($5^{12}6^2$) and small (5^{12}) cages of sI hydrate, respectively (Ota et al., 2007).

The cage occupancy ratios (θ_l/θ_s) for enclathrated CH_4 molecules can also be determined from the relative areas of the corresponding Raman peaks (CH_4 hydrate: 1.07 (Mok et al., 2020), NGH at AM03: 1.03, NGH at AM06: 1.01). As was observed from ^{13}C NMR measurement, the NGHs at both AM03 and AM06 had slightly smaller θ_l/θ_s values than that of CH_4 hydrate, which indicates the possible incorporation of other guest molecules besides CH_4. The Raman spectra demonstrated that H_2S was clearly encapsulated in the hydrate cages and the inclusion of H_2S could slightly alter the guest distributions of NGHs.

Even though ^{13}C NMR and Raman analyses enable us to estimate the gas hydrate structure from the positions of cage-dependent peaks for specific guest molecules, the accurate information about the crystalline structure and lattice parameters of gas hydrates can be obtained by profile matching analysis of PXRD patterns. In addition, quantitative analysis via Rietveld refinement can reveal the weight fractions of each structure and cage occupancy of guest molecules in gas hydrates (Takeya et al., 2010). The PXRD patterns of the NGHs at AM03 and AM06 are presented in Fig. 5, and their summarized crystalline information is listed in Table 2. The NGHs at both AM03 and AM06 were identified as cubic sI ($Pm\overline{3}n$) with lattice parameters of a = 11.8788(2) Å and a = 11.8654(1) Å, respectively. The lattice parameters of the NGHs at AM03 and AM06 were quite similar to each other, and also similar to that of CH_4 hydrate (a = 11.8822 Å) (Mok et al., 2020). This also implies that the NGHs at AM03 and AM06 are composed mainly of CH_4 as guest molecules.

Because GC and Raman analyses demonstrated that the NGHs at AM03 and AM06 possessed CH_4 and H_2S as guest molecules, the weight fractions of sI and hexagonal ice (Ih) and the cage occupancy values of CH_4 and H_2S were calculated via Rietveld refinement using the FullProf program. As shown in Table 2, the NGHs at both AM03 and AM06 had similar cage occupancy values of CH_4 and H_2S. The weight fractions of sI were ~36% for the NGH at AM03 and ~36% for the NGH at AM06. The PXRD patterns clearly indicated that the NGHs at AM03 and AM06 are very similar in the crystalline structure, guest compositions, and hydrate saturation and that they exist in a similar environment and surroundings for gas hydrate formation.

To examine the influence of hydrate formation on salinity in the pore water of the sediment, the salt contents in the seawater, sediment, and hydrate phase were separately measured in this study because salinity can directly affect the thermodynamic stability of NGHs. Fig. 6 (a) presents the measured salinity of each phase (hydrate and sediment) of the NGH at AM06. The salinity of residual pore water in the hydrate-bearing sediment was found to be 50.32‰, which was much higher than that of seawater (34.88‰). An extremely low salinity was observed in the hydrate phase, which was possibly caused by the presence of remaining salts that were not completely excluded from the hydrate phase. In this study, the salinity in the residual pore water of the hydrate-bearing sediment was abnormally high even though several

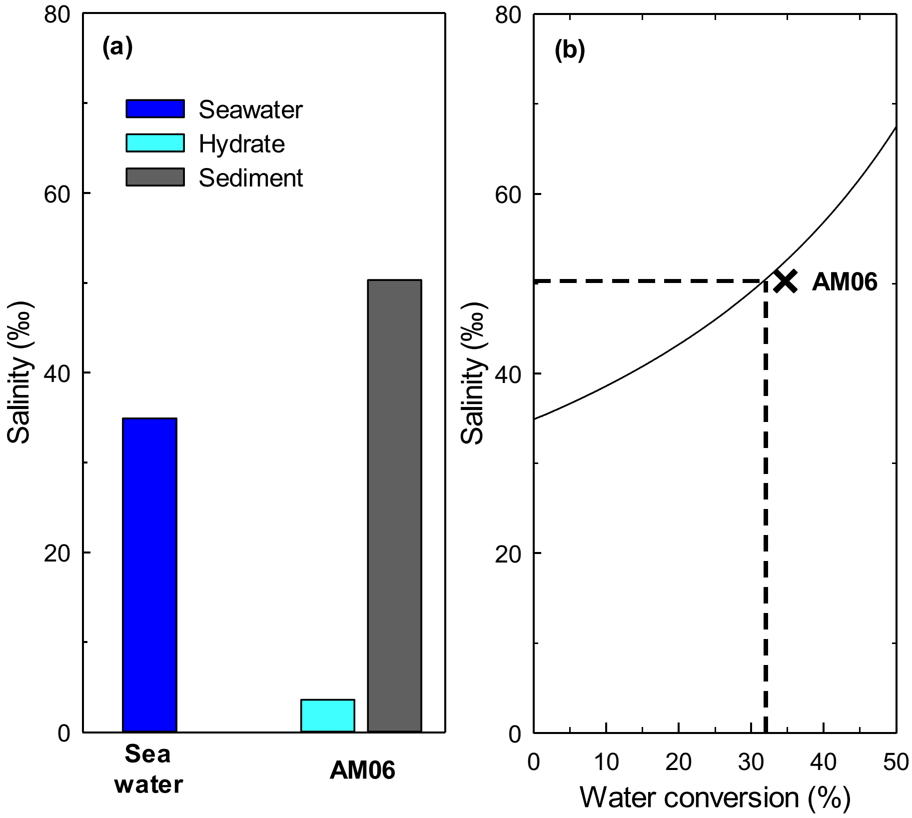

Fig. 6. (a) Salinity of NGH at AM06, and (b) changes in the salinity of pore water depending on water conversion.

previous studies have reported that the salinity of pore water in the sediment of the Arctic region was similar to that of seawater (Chen et al., 2016; Chen et al., 2017). This abnormal salinity enrichment is conjectured to occur in hydrate-bearing sediment with extremely low permeability.

Assuming that the pores of the sediment were initially filled with seawater with a salinity of 34.88‰, the salinity of pore water would be concentrated as the conversion of water to NGHs progressed. In addition, because the low-permeability sediment containing fine grains and gas hydrates was assumed to constitute a closed system, the movement of salts out of the system was ignored (Chuvilin et al., 2021; Yang and Aplin, 2010). Based on the above assumptions, the salinity of residual pore water was calculated to be 50.32‰ when 32% of the initial water was converted to NGHs as depicted in Fig. 6(b). The value of hydrate conversion (32%) was in remarkable agreement with that of hydrate fraction (~36%) obtained from the quantitative analysis of the PXRD patterns (marked as a black cross in Fig. 6(b)). This means that the limited mass transfer caused by the low permeability of sediment can induce the enrichment of salinity in the residual pore water; therefore, the NGHs in the mass transfer-limited sediment can be less thermodynamically stable than expected due to the enhanced thermodynamic inhibition effect caused by the enriched salinity.

Because all ARAON Mounds have gas chimney structures as confirmed by the sub-bottom profile and the saturation of the NGHs at AM03 and AM06 was found to be similar, it was reasonably assumed that NGHs could exist in all ARAON Mounds and that the saturation of NGHs at all ARAON Mounds was the same (Kim et al., 2020a; Kim et al., 2020b). With these assumptions, the temperature buffers for dissociation of NGHs (ΔT)—referring to the temperature gaps between the hydrate phase equilibria and the existing conditions of the NGHs—were calculated to examine the effect of the temperature rise of seawater caused by global warming on the thermodynamic stability of the NGHs. Fig. 7(a) shows the thermodynamic conditions of each ARAON Mound obtained from CTD and the phase equilibria of CH_4 hydrates both in seawater and salt-enriched pore water calculated by CSMGEM. In this study, CTD values were used as the temperature and pressure conditions of the NGHs. The additional thermodynamic inhibition caused by the salt enrichment in pore water of the hydrate-bearing sediment was quantified and the resulting ΔT values at each ARAON Mound are shown in Fig. 7(b). Since the CTD results showed that the temperature and salinity at each ARAON Mound were almost the same, the most significant factor in determining the thermodynamic stability of the NGHs was the hydraulic pressure. Therefore, the ΔT for dissociation of the NGHs decreased as the depth of the Mound became shallower. In addition, the calculated ΔT values based on the phase equilibria of the CH_4 + NaCl (50.32‰) hydrate indicated that the NGHs at ARAON Mounds could start to dissociate at a temperature ~ 1 K lower than the expected temperature based on the salinity of seawater (34.88‰).

Although the enriched salinity in pore water makes the NGH dissociation in the sediment start to occur at a lower temperature than expected, the salinity in the pore water will eventually be recovered to that of the surroundings (34.88‰) as the NGH dissociation progresses. To understand the potential CH_4-releasing phenomenon that might be caused by the NGH dissociation, the changes in both ΔT and gas hydrate saturation depending on the salinity and seawater temperature were calculated on the basis of hydrate phase equilibria and mass balance (Fig. 8). As shown in Fig. 8(a), the ΔT values of the NGHs at all Mounds gradually increased with a decrease in salinity. At deeper Mounds, the slope of the line (ΔT versus salinity) was slightly steeper, because the equilibrium temperature shift due to the thermodynamic inhibition effect of NaCl was more significant at higher pressures as shown in Fig. 7(a). This indicates that the salt enrichment in the sediment at deeper Mounds has a slightly greater impact on the change in ΔT. In Fig. 8(b), the changes in the saturation of NGHs at ARAON Mounds were predicted by the shifts of hydrate phase equilibria depending on the seawater temperature and salinity. The dissociation of NGHs will start to occur sequentially from the NGH at a shallower Mound to the NGH at a deeper one as the seawater temperature rises. During the dissociation of NGHs, the saturation of NGHs will continuously decrease and accordingly, the phase equilibria of NGHs will also continuously shift due to the dilution of pore water and the consequent lowered salinity. Therefore, as seen in Fig. 8(b), the temperature at which the dissociation of NGHs ends was higher than that at which the NGHs start to dissociate. This temperature difference was slightly larger for NGHs at deeper Mounds.

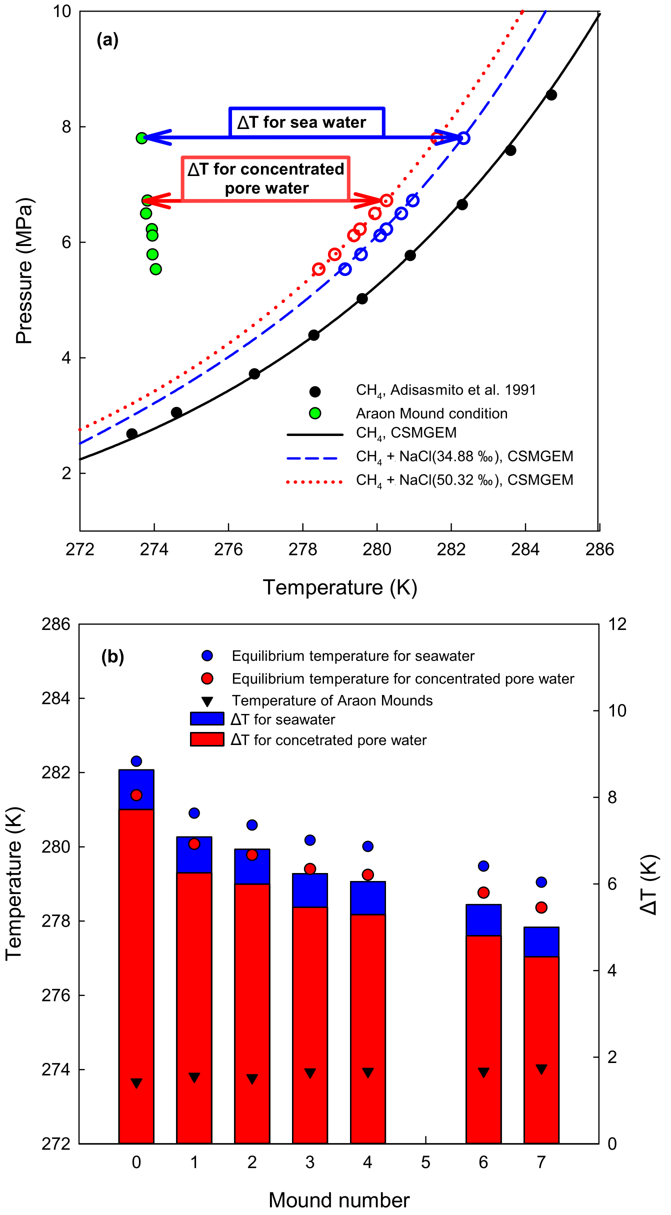

Fig. 7. (a) Phase equilibria of CH_4 + NaCl hydrates and thermodynamic conditions of NGHs at ARAON Mounds (Adisasmito et al., 1991), and (b) calculated temperature buffers for dissociation of NGHs (ΔT) with seawater and concentrated pore water.

4. Conclusions

In this study, the analyses of NGH samples (NGHs at AM03 and AM06) retrieved from ARAON Mounds in the Chukchi Sea using various analytical instruments, the measurement and prediction of the salinity in pore water of the hydrate-bearing sediments, and the impact of the salt-enrichment on the thermodynamic stability of NGHs at ARAON

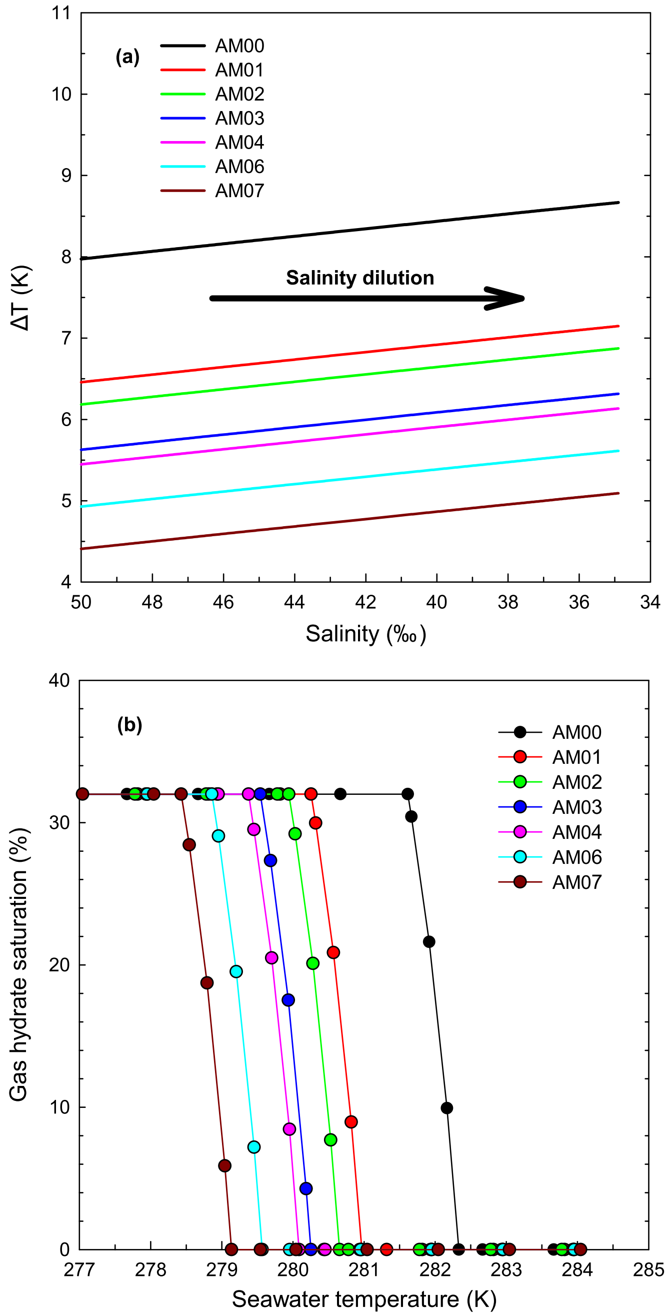

Fig. 8. (a) Changes in ΔT depending on salinity, and (b) changes in gas hydrate saturation depending on seawater temperature.

Mounds were closely investigated. Although the GC analysis indicated the inclusion of mostly CH_4 and small fractions of H_2S and CO_2 in the NGHs at AM03 and AM06, it was found from ^{13}C NMR and Raman spectroscopic results that both CH_4 and H_2S were enclathrated in small (5^{12}) and large ($5^{12}6^2$) cages of sI hydrate, and that CO_2 might reside in the residual water. The profile matching and Rietveld refinement of the PXRD patterns demonstrated that the NGHs at AM03 and AM06 were similar in the weight fractions of sI and Ih and the cage occupancy of CH_4 and H_2S to each other, which implies that they exist in a similar environment and surroundings for gas hydrate formation. The salinity in residual pore water of the hydrate-bearing sediment (AM06) was abnormally high (50.32‰). This indicates that the salinity of the residual pore water in the hydrate-bearing sediment with low permeability can be enriched due to the limited mass transfer. From the predicted temperature buffers for dissociation of NGHs (ΔT), it is postulated that the dissociation of the NGHs at ARAON Mounds could start to occur at a temperature ~ 1 K lower than expected due to the enhanced thermodynamic inhibition effect at the higher salinity. As the dissociation of NGHs progressed, the saturation of NGHs would continuously decrease and the salinity of the pore water would eventually recover to that of seawater. Therefore, the temperature at which the NGH dissociation terminates was higher than that at which the NGHs begin to dissociate. This study not only experimentally examined the thermodynamic characteristics of NGHs but also revealed the possible dissociation of NGHs at a lower temperature than expected due to the enriched salinity in the hydrate-bearing sediments. The results will be useful and meaningful as fundamental key information for exploring and exploiting NGHs in Arctic regions and understanding the potential CH_4-releasing phenomenon that might be caused by global warming.

CRediT authorship contribution statement

Wonjung Choi: Conceptualization, Writing – original draft, Investigation, Formal analysis, Validation, Visualization. **Joonseop Lee:** Writing – original draft, Investigation, Validation, Visualization. **Young-Gyun Kim:** Investigation, Formal analysis, Visualization. **Hanwoong Kim:** Conceptualization, Formal analysis, Validation. **Tae Siek Rhee:** Investigation, Formal analysis, Validation. **Young Keun Jin:** Formal analysis, Validation, Project administration. **Ji-Hoon Kim:** Investigation, Validation. **Yongwon Seo:** Supervision, Validation, Writing – review & editing, Project administration.

Declaration of competing interest

The authors declare that they have no known competing financial interests or personal relationships that could have appeared to influence the work reported in this paper.

Acknowledgements

This work was supported by the KIMST Grant (1525011795) and by the National Research Foundation of Korea (NRF) (No. 2019R1A6A1A03033167, No. 2020R1C1C1007495, and No. 2021R1A2C2005856).

References

Adisasmito, S., Frank III, R.J., Sloan, E.D., 1991. Hydrates of carbon dioxide and methane mixtures. J. Chem. Eng. Data 36, 68–71.

Almenningen, S., Iden, E., Fernø, M.A., Ersland, G., 2018. Salinity effects on pore-scale methane gas hydrate dissociation. J. Geophys. Res. Solid Earth 123, 5599–5608.

Bahk, J.J., Kim, D.H., Chun, J.H., Son, B.K., Kim, J.H., Ryu, B.J., Torres, M.E., Riedel, M., Schultheiss, P., 2013. Gas hydrate occurrences and their relation to host sediment properties: results from second Ulleung Basin gas hydrate drilling expedition, East Sea. Mar. Pet. Geol. 47, 21–29.

Biastoch, A., Treude, T., Rüpke, L.H., Riebesell, U., Roth, C., Burwicz, E.B., Park, W., Latif, M., Böning, C.W., Madec, G., Wallmann, K., 2011. Rising Arctic Ocean temperatures cause gas hydrate destabilization and ocean acidification. Geophys. Res. Lett. 38.

Chen, L., Lu, H., Ripmeester, J.A., 2015. Dissociation conditions and raman spectra of CO2 SO2 and CO2 H2S hydrates. Ind. Eng. Chem. Res. 54, 5543–5549.

Chen, M., Kim, J.-H., Nam, S.-I., Niessen, F., Hong, W.-L., Kang, M.-H., Hur, J., 2016. Production of fluorescent dissolved organic matter in Arctic Ocean sediments. Sci. Rep. 6, 39213.

Chen, M., Nam, S.-I., Kim, J.-H., Kwon, Y.-J., Hong, S., Jung, J., Shin, K.-H., Hur, J., 2017. High abundance of protein-like fluorescence in the Amerasian Basin of Arctic Ocean: potential implication of a fall phytoplankton bloom. Sci. Total Environ. 599–600, 355–363.

Choi, W., Lee, Y., Mok, J., Lee, S., Lee, J.D., Seo, Y., 2019. Thermodynamic and kinetic influences of NaCl on HFC-125a hydrates and their significance in gas hydrate-based desalination. Chem. Eng. J. 358, 598–605.

Choi, W., Go, W., Lee, Y., Mok, J., Seo, Y., 2020a. Mechanism and kinetics of guest exchange in sII hydrate – flue gas replacement as revealed by experimental and computational approaches for hydrocarbon recovery and CO2 sequestration. Chem. Eng. J. 417, 128119.

Choi, W., Lee, Y., Mok, J., Seo, Y., 2020b. Influence of feed gas composition on structural transformation and guest exchange behaviors in sH hydrate – flue gas replacement for energy recovery and CO2 sequestration. Energy 207, 118299.

Chuvilin, E., Grebenkin, S., Zhmaev, M., 2021. Gas permeability of sandy sediments: effects of phase changes in pore ice and gas hydrates. Energy Fuel 35, 7874–7882.

Dickens, G.R., Quinby-Hunt, M.S., 1994. Methane hydrate stability in seawater. Geophys. Res. Lett. 21, 2115–2118.

Fang, Y., Wei, J., Lu, H., Liang, J., Lu, J.A., Fu, J., Cao, J., 2019. Chemical and structural characteristics of gas hydrates from the Haima cold seeps in the Qiongdongnan Basin of the South China Sea. J. Asian Earth Sci. 182, 103924.

Gamboa, A., Montero-Serrano, J.-C., St-Onge, G., Rochon, A., Desiage, P.-A., 2017. Mineralogical, geochemical, and magnetic signatures of surface sediments from the Canadian Beaufort shelf and Amundsen gulf (Canadian Arctic). Geochem. Geophys. Geosyst. 18, 488–512.

Gründger, F., Carrier, V., Svenning, M.M., Panieri, G., Vonnahme, T.R., Klasek, S., Niemann, H., 2019. Methane-fuelled biofilms predominantly composed of methanotrophic ANME-1 in Arctic gas hydrate-related sediments. Sci. Rep. 9, 9725.

Hahm, D., Baker, E.T., Rhee, T., Won, Y.-J., Resing, J.A., Lupton, J.E., Lee, W.-K., Kim, M., Park, S.-H., 2015. First hydrothermal discoveries on the australian-Antarctic ridge: discharge sites, plume chemistry, and vent organisms. Geochem. Geophys. Geosyst. 16, 3061–3075.

Holder, G.D., Malone, R.D., Lawson, W.F., 1987. Effects of gas composition and geothermal properties on the thickness and depth of natural-gas-hydrate zones. J. Pet. Tech. 39, 1147–1152.

Hong, W.-L., Torres, M.E., Carroll, J., Crémière, A., Panieri, G., Yao, H., Serov, P., 2017. Seepage from an Arctic shallow marine gas hydrate reservoir is insensitive to momentary ocean warming. Nat. Commun. 8, 15745.

Jin, Y., Konno, Y., Yoneda, J., Kida, M., Nagao, J., 2016. In situ methane hydrate morphology investigation: natural gas hydrate-bearing sediment recovered from the eastern nankai trough area. Energy Fuel 30, 5547–5554.

Kim, J.-H., Torres, M.E., Hong, W.-L., Choi, J., Riedel, M., Bahk, J.-J., Kim, S.-H., 2013. Pore fluid chemistry from the second gas hydrate drilling expedition in the Ulleung Basin (UBGH2): source, mechanisms and consequences of fluid freshening in the central part of the Ulleung Basin, East Sea. Mar. Pet. Geol. 47, 99–112.

Kim, S., Baek, I.-H., You, J.K., Seo, Y., 2016. Phase equilibria, dissociation enthalpies, and raman spectroscopic analyses of N2 tetra-n-butyl ammonium chloride (TBAC) semiclathrates. Fluid Phase Equilib. 413, 86–91.

Kim, J.-H., Hachikubo, A., Kida, M., Minami, H., Lee, D.-H., Jin, Y.K., Ryu, J.-S., Lee, Y.M., Hur, J., Park, M.-H., Kim, Y.-G., Kang, M.-H., Park, S., Chen, M., Kang, S.-G., Kim, S., 2020a. Upwarding gas source and postgenetic processes in the shallow sediments from the ARAON mounds, Chukchi Sea. J. Nat. Gas. Sci. Eng. 76, 103223.

Kim, Y.-G., Kim, S., Lee, D.-H., Lee, Y.M., Kim, H.J., Kang, S.-G., Jin, Y.K., 2020b. Occurrence of active gas hydrate mounds in the southwestern slope of the Chukchi Plateau, Arctic Ocean. Episodes: J. Int. Geosci. 43, 811–823.

Klapp, S.A., Murshed, M.M., Pape, T., Klein, H., Bohrmann, G., Brewer, P.G., Kuhs, W.F., 2010. Mixed gas hydrate structures at the chapopote knoll, southern Gulf of Mexico. Earth Planet. Sci. Lett. 299, 207–217.

Kvenvolden, K.A., Lorenson, T.D., 2001. The Global Occurrence of Natural Gas Hydrate, Natural Gas Hydrates: Occurrence, Distribution, and Detection, pp. 3–18.

Lee, S., Park, S., Lee, Y., Seo, Y., 2013. Thermodynamic and 13C NMR spectroscopic verification of methane–carbon dioxide replacement in natural gas hydrates. Chem. Eng. J. 225, 636–640.

Lee, Y., Choi, W., Shin, K., Seo, Y., 2017. CH4-CO2 replacement occurring in sII natural gas hydrates for CH4 recovery and CO2 sequestration. Energy Convers. Manag. 150, 356–364.

Lee, J., Lee, D., Seo, Y., 2021b. Experimental investigation of the exact role of large-molecule guest substances (LMGSs) in determining phase equilibria and structures of natural gas hydrates. Energy 215, 119219.

Li, J.-F., Ye, J.-L., Qin, X.-W., Qiu, H.-J., Wu, N.-Y., Lu, H.-L., Xie, W.-W., Lu, J.-A., Peng, F., Xu, Z.-Q., Lu, C., Kuang, Z.-G., Wei, J.-G., Liang, Q.-Y., Lu, H.-F., Kou, B.-B., 2018. The first offshore natural gas hydrate production test in South China Sea. China Geol. 1, 5–16.

Lu, H., Seo, Y.-T., Lee, J.-W., Moudrakovski, I., Ripmeester, J.A., Chapman, N.R., Coffin, R.B., Gardner, G., Pohlman, J., 2007. Complex gas hydrate from the Cascadia margin. Nature 445, 303–306.

MacDougall, A.H., Avis, C.A., Weaver, A.J., 2012. Significant contribution to climate warming from the permafrost carbon feedback. Nat. Geosci. 5, 719–721.

Marín-Moreno, H., Giustiniani, M., Tinivella, U., Piñero, E., 2016. The challenges of quantifying the carbon stored in Arctic marine gas hydrate. Mar. Pet. Geol. 71, 76–82.

Maslin, M., Owen, M., Betts, R., Day, S., Dunkley Jones, T., Ridgwell, A., 2010. Gas hydrates: past and future geohazard? Philos. Trans. R. Soc. A 368, 2369–2393.

Max, M.D., Johnson, A.H., Dillon, W.P., 2013. Estimates of the NGH Resource Base in the Arctic Region, Natural Gas Hydrate - Arctic Ocean Deepwater Resource Potential. Springer International Publishing, Cham, pp. 85–89.

Mok, J., Choi, W., Seo, Y., 2020. Time-dependent observation of a cage-specific guest exchange in sI hydrates for CH4 recovery and CO2 sequestration. Chem. Eng. J. 389, 124434.

Mok, J., Choi, W., Seo, Y., 2021. Evaluation of kinetic salt-enrichment behavior and separation performance of HFC-152a hydrate-based desalination using an experimental measurement and a thermodynamic correlation. Water Res. 193, 116882.

Ota, M., Saito, T., Aida, T., Watanabe, M., Sato, Y., Smith Jr., R.L., Inomata, H., 2007. Macro and microscopic CH4–CO2 replacement in CH4 hydrate under pressurized CO2. AIChE J. 53, 2715–2721.

Pape, T., Bünz, S., Hong, W.-L., Torres, M.E., Riedel, M., Panieri, G., Lepland, A., Hsu, C.-W., Wintersteller, P., Wallmann, K., Schmidt, C., Yao, H., Bohrmann, G., 2020. Origin and transformation of light hydrocarbons ascending at an active pockmark on Vestnesa Ridge, Arctic Ocean. J. Geophys. Res. Solid Earth 125, e2018JB016679.

Peltzer, E.T., Zhang, X., Walz, P.M., Luna, M., Brewer, P.G., 2016. In situ raman measurement of HS- and H2S in sediment pore waters and use of the HS-:H2S ratio as an indicator of pore water pH. Mar. Chem. 184, 32–42.

Pinero, E., Marquardt, M., Hensen, C., Haeckel, M., Wallmann, K., 2013. Estimation of the global inventory of methane hydrates in marine sediments using transfer functions. Biogeosciences 10, 959.

Ruppel, C., Dickens, G.R., Castellini, D.G., Gilhooly, W., Lizarralde, D., 2005. Heat and salt inhibition of gas hydrate formation in the northern Gulf of Mexico. Geophys. Res. Lett. 32.

Sahu, C., Kumar, R., Sangwai, J.S., 2020. Comprehensive review on exploration and drilling techniques for natural gas hydrate reservoirs. Energy Fuel 34, 11813–11839.

Seo, Y.-T., Lee, H., 2003. 13C NMR analysis and gas uptake measurements of pure and mixed gas hydrates: development of natural gas transport and storage method using gas hydrate. Korean J. Chem. Eng. 20, 1085–1091.

Serov, P., Vadakkepuliyambatta, S., Mienert, J., Patton, H., Portnov, A., Silyakova, A., Panieri, G., Carroll, M.L., Carroll, J., Andreassen, K., Hubbard, A., 2017. Postglacial response of Arctic Ocean gas hydrates to climatic amelioration. PNAS 114, 6215–6220.

Sloan, E.D., Koh, C.A., 2007. Clathrate Hydrates of Natural Gases. 3rd ed. CRC press.

Stern, L.A., Lorenson, T.D., Pinkston, J.C., 2011. Gas hydrate characterization and grain-scale imaging of recovered cores from the mount Elbert gas hydrate stratigraphic test well, Alaska north slope. Mar. Pet. Geol. 28, 394–403.

Takeya, S., Udachin, K.A., Moudrakovski, I.L., Susilo, R., Ripmeester, J.A., 2010. Direct space methods for powder X-ray diffraction for guest-host materials: applications to cage occupancies and guest distributions in clathrate hydrates. J. Am. Chem. Soc. 132, 524–531.

Uchida, T., Takagi, A., Kawabata, J., Mae, S., Hondoh, T., 1995. Raman spectroscopic analyses of the growth process of CO2 hydrates. Energy Convers. Manag. 36, 547–550.

Wallmann, K., Riedel, M., Hong, W.L., Patton, H., Hubbard, A., Pape, T., Hsu, C.W., Schmidt, C., Johnson, J.E., Torres, M.E., Andreassen, K., Berndt, C., Bohrmann, G., 2018. Gas hydrate dissociation off Svalbard induced by isostatic rebound rather than global warming. Nat. Commun. 9, 83.

Wei, J., Fang, Y., Lu, H., Lu, H., Lu, J., Liang, J., Yang, S., 2018. Distribution and characteristics of natural gas hydrates in the Shenhu Sea area, South China Sea. Mar. Pet. Geol. 98, 622–628.

Wei, J., Liang, J., Lu, J., Zhang, W., He, Y., 2019. Characteristics and dynamics of gas hydrate systems in the northwestern South China Sea - results of the fifth gas hydrate drilling expedition. Mar. Pet. Geol. 110, 287–298.

Wei, J., Wu, T., Zhu, L., Fang, Y., Liang, J., Lu, H., Cai, W., Xie, Z., Lai, P., Cao, J., Yang, T., 2021. Mixed gas sources induced co-existence of sI and sII gas hydrates in the Qiongdongnan Basin, South China Sea. Mar. Pet. Geol. 128, 105024.

Wu, T., Deng, X., Yao, H., Liu, B., Ma, J., Waseem Haider, S., Yu, Z., Wang, L., Yu, M., Lu, J., Naimatullah Sohoo, E., Ahmed Kalhoro, N., Kahkashan, S., Wei, J., 2021. Distribution and development of submarine mud volcanoes on the makran continental margin, offshore Pakistan. J. Asian Earth Sci. 207, 1–7.

Yang, Y., Aplin, A.C., 2010. A permeability–porosity relationship for mudstones. Mar. Pet. Geol. 27, 1692–1697.

Ye, J., Wei, J., Liang, J., Lu, J., Lu, H., Zhang, W., 2019. Complex gas hydrate system in a gas chimney, South China Sea. Mar. Pet. Geol. 104, 29–39.